Environmental Science & Technology
pubs.acs.org/est
Article

Pyro-Catalytic Degradation of Pyrene by Bentonite-Supported Transition Metals: Mechanistic Insights and Trade-Offs with Low Pyrolysis Temperature

Sara B. Denison, Peixuan Jin, Priscilla Dias Da Silva, Chun Chu, Bhagavatula Moorthy, Thomas P. Senftle, Kyriacos Zygourakis,* and Pedro J. J. Alvarez*

Cite This: *Environ. Sci. Technol.* 2023, 57, 14373−14383

Read Online

ACCESS | Metrics & More | Article Recommendations | Supporting Information

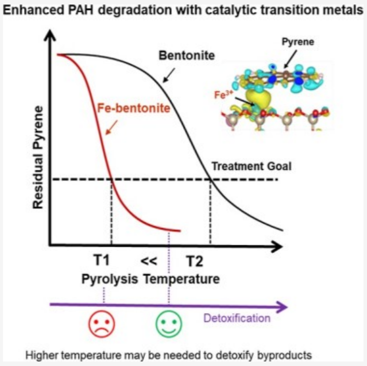

ABSTRACT: Transition metal catalysts can significantly enhance the pyrolytic remediation of soils contaminated with polycyclic aromatic hydrocarbons (PAHs). Significantly higher pyrene removal efficiency was observed after the pyrolytic treatment of Fe-enriched bentonite (1.8% wt ion-exchanged content) relative to natural bentonite or soil (i.e., 93% vs 48% and 4%) at the unprecedentedly low temperature of 150 °C with only 15 min treatment time. DFT calculations showed that bentonite surfaces with Fe^{3+} or Cu^{2+} adsorb pyrene stronger than surfaces with Zn^{2+} or Na^+. Enhanced pyrene adsorption results from increased charge transfer from its aromatic π-bonds to the cation site, which destabilizes pyrene allowing for faster degradation at lower temperatures. UV−Vis and GC−MS analyses revealed pyrene decomposition products in extracts of samples treated at 150 °C, including small aromatic compounds. As the pyrolysis temperature increased above 200 °C, product distribution shifted from extractable compounds to char coating the residue particles. No extractable byproducts were detected after treatment at 400 °C, indicating that char was the final product of pyrene decomposition. Tests with human lung cells showed that extracts of samples pyrolyzed at 150 °C were toxic; thus, high removal efficiency by pyrolytic treatment does not guarantee detoxification. No cytotoxicity was observed for extracts from Fe-bentonite samples treated at 300 °C, inferring that char is an appropriate treatment end point. Overall, we demonstrate that transition metals in clay can catalyze pyrolytic reactions at relatively low temperatures to decrease the energy and contact times required to meet cleanup standards. However, mitigating residual toxicity may require higher pyrolysis temperatures.

KEYWORDS: *pyrolysis, catalysis, PAHs, clays, soil remediation, residual toxicity*

INTRODUCTION

Environmental contamination by polycyclic aromatic hydrocarbons (PAHs) poses a major threat to public health due to their classification as possible and probable carcinogens by the US EPA and their link to preterm births.[1−3] These compounds tend to persist in the environment due to their hydrophobic and semi-volatile properties and their resistance to biodegradation.[1,4]

Pyrolysis is an effective thermal treatment method that can rapidly and reliably remove PAHs and other toxic hydrophobic organic pollutants to meet soil cleanup standards without destroying soil fertility to facilitate re-greening efforts.[5−7] Working with soils contaminated with weathered petroleum crudes, we demonstrated that pyrolytic treatment could remove total petroleum hydrocarbons (TPH) (13,000 to 19,000 mg/kg) by more than 99.9% at temperatures between 420 and 470 °C.[6,7] Pyrolytic treatment at 420 °C also removed more than 98% of the 16 EPA-regulated PAHs present in the hydrocarbon contaminants and effectively detoxified the soil as determined by cell viability tests.[7] Other investigators showed that amending petroleum and PAH-contaminated soils with materials like hematite, K_2CO_3, CaO, red mud, or redox-active minerals can enhance TPH removal via pyrolytic treatment.[8−12] Although the pyrolytic treatment temperatures commonly used in previous studies (400−500 °C)[13] are lower than those required for incineration and other thermal treatment methods (600−1200 °C),[14] the relatively high energy requirements remain a major cost-driver for the pyrolytic treatment method and a sustainability challenge.[15−17] Recently, we showed that natural clays and clays impregnated with earth-abundant transition metals (e.g., Fe or Cu) can catalyze pyrolysis reactions and decrease the treatment temperature required for high hydrocarbon removal from petroleum-contaminated soils.[18] Although clays with their natural exchangeable cations were effective catalysts, we

Received: June 12, 2023
Revised: August 21, 2023
Accepted: August 25, 2023
Published: September 8, 2023

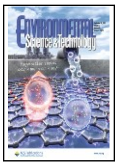

https://doi.org/10.1021/acs.est.3c04487

Table 1. Total Metal Content in Bentonite and Metal Ion-Exchanged Bentonite Samples

Sample (% wt)	Natural Bentonite	Fe-Bentonite	Cu-Bentonite	Zn-Bentonite
Al	1.01 ± 0.328	1.05 ± 0.005	0.900 ± 0.016	0.914 ± 0.017
Cu	N.D.[a]	N.D.	3.48 ± 0.043	N.D.
K	0.637 ± 0.057	0.158 ± 0.029	0.343 ± 0.055	N.D.
Fe	2.93 ± 0.791	4.76 ± 0.0810	2.03 ± 0.057	2.18 ± 0.095
Mg	1.022 ± 0.324	0.818 ± 0.002	0.783 ± 0.022	0.818 ± 0.02
Na	0.796 ± 0.585	N.D.	0.478 ± 0.013	N.D.
Zn	N.D.	N.D.	N.D.	2.13 ± 0.025

[a] N.D.: not detected (LOD ∼ 1−100 ppt).

achieved significantly higher hydrocarbon removal at lower pyrolysis temperatures using clays with ion-exchanged Fe or Cu.[18] By amending the contaminated soil with 10% wt bentonite (a natural clay) impregnated with Fe, for example, we achieved 93% TPH removal efficiency at the relatively low pyrolysis temperature of 300 °C.[18] We postulated that the catalytic mechanism involved π−cation interactions between the large aromatic compounds of petroleum crudes and transition metals present in the amendments. These interactions start a cascade of reactions that convert large aromatics into inert char, which is an acceptable, safe treatment endpoint. However, this work studied the pyrolysis of a complex mixture of petroleum hydrocarbons and did not directly show that transition metals catalyze the decomposition of PAH molecules, which are a major toxicity driver in petroleum-contaminated sites.

Pyrene has been used in previous studies as a model compound to study the thermal decomposition of PAHs. Homogeneous (gas phase) pyrolysis of pyrene requires very high temperatures (900−1200 °C) to trigger cyclo-dehydrogenation and polymerization reactions that form bi-pyrenes, larger condensation products, and eventually soot or char.[19] Working with pyrene-contaminated soil, several studies reported that complete pyrene degradation required heating the soil to 530 °C at heating rates faster than 100 °C/s under helium flow.[20,21] Excess soil weight loss and increased CO and CO_2 yields were observed above 500 °C, suggesting that chemical reactions of soil components with pyrene decomposition products took place under these conditions. However, potential catalytic reactions mediated by transition metals in clays to facilitate the thermal treatment of pyrene or other PAHs in contaminated soils remain largely unexplored.

This present study demonstrates that bentonite impregnated with selected ion-exchanged transition metals (Fe, Cu, and Zn) catalyzes the decomposition of pyrene and achieves high conversions at temperatures as low as 150 °C with Fe or Cu. Catalysis by earth-abundant transition metals deposited on clay allows pyrolytic treatment of PAH-contaminated soils to proceed at lower temperatures than those reported in the current literature. This would decrease the energy requirements and, thus, the operating costs and carbon footprint of our thermal remediation process. However, it is important to consider the unintended consequences of pyrolytic treatment at the unprecedentedly low pyrolysis temperatures made possible by these catalysts. To inform the cost-effective and safe application of the pyro-catalytic treatment, this study also provides insights into the mechanisms mediated by different transition metals and assesses the toxicity of the pyrolysis products obtained at different temperatures.

MATERIALS AND METHODS

Materials. Pure bentonite (Sigma-Aldrich) was used as a reference clay to prepare metal-impregnated clays. Anhydrous iron (III) nitrate (nonahydrate, >98%), copper (II) nitrate (hemi(pentahydrate), >98%), and zinc (II) nitrate (hexahydrate, >98%) were obtained from Sigma-Aldrich. Pyrene (98%) was purchased from Sigma-Aldrich. All chemicals were used as received. Uncontaminated soil (composed of 37% sand, 20% silt, and 43% clay) was collected from Rice University in Houston, TX. The collected soil was dried at 60 °C for 72 h to prevent oxidation and changes in the amount of organic matter in the sample,[22,23] homogenized, and sieved (<1 mm) to remove large particles.

Preparation and Characterization of Ion-Exchanged Bentonites. The preparation of the ion-exchanged clays was modified slightly from our past work.[18] Briefly, bentonite was modified by liquid-phase ion-exchange to obtain Fe-bentonite, Cu-bentonite, or Zn-bentonite. Fe, Cu, and Zn were chosen because they are metals commonly found in soils and represent a range of redox potentials (Table S1). To create the modified ion-exchanged clays, 20 g of bentonite was added to 400 mL of 0.6 N Fe(III), Cu(II), or Zn(II) solutions. The mixture was covered with parafilm and stirred at 300 rpm for 24 h at room temperature. After stirring, the mixture was filtered and dried at 105 °C for 24 h. The modified-bentonite clays were then ground using a mortar and pestle and sieved (mesh N° 60, <250 μm). Samples were stored at room temperature in capped glass vials. The metal content of the pure bentonite and modified bentonite with Fe, Cu, or Zn (Table 1) was determined by an inductively coupled plasma (ICP) method using a Perkin Elmer Optima DRC II ICP−MS (Mississippi State Chemical Laboratory, Starkville, MS). As we also observed in our previous work using ion-exchanged clays,[18] the ion-exchange process replaced alkali and alkali-earth cations of the pure bentonite with iron, copper, and zinc cations.

Surface area measurements were determined using the BET method (Quantachrome Autosorb-iQ-MP/Kr BET Surface Analyzer). The specific surface areas for bentonite, Fe-bentonite, Cu-bentonite, and Zn-bentonite were 34.69, 46.60, 46.10, and 42.03 m^2/g, respectively.

Bentonite and ion-exchanged bentonite clays were spiked with pyrene at 0.1% wt. The samples were prepared by mixing 1 g of bentonite or cation-modified bentonite (Fe, Cu, or Zn) with 2 mL of a solution containing 0.5 mg/mL of pyrene in HPLC-grade acetone solvent. The clay and pyrene mixture was stirred and stored at room temperature until acetone was completely evaporated. The final pyrene concentration was 1000 mg/kg or 0.1% wt. The soil used for our benchmarking experiments was also spiked with pyrene at 0.1% wt using the same procedure.

The treated and untreated clays were characterized by X-ray photoelectron spectroscopy (XPS) using a Quantera X-ray photoelectron spectrometer (Physical Electronics, Inc., Chanhassen, MN) to determine the elemental state of the clay surface (1−10 nm). Samples were calibrated and shifted using 284.5 eV as the standard carbon binding energy. The X-ray source was an aluminum anode with a pass energy of 26 eV. Iron was examined from 704 to 720 eV with 60 sweeps and copper from 930 to 940 eV with 60 sweeps. MultiPak (Physical Electronics) software was used for data analysis and curve fitting.

Pyrolytic Treatment of Contaminated Clays. Pyrolysis experiments were performed using a thermogravimetric analyzer (TGA) (Q500, TA Instruments, New Castle, DE). For all pyrolysis experiments, 200 mg of each pyrene-contaminated clay sample was placed in an alumina pan and treated in the TGA under high-purity nitrogen flowing at 100 mL/min. After equilibrating the sample at 27 °C for 30 min, the temperature was ramped at 50 °C/min to the desired pyrolysis temperature (150, 200, 300, or 400 °C) and held there for 15 min before cooling down to room temperature. While the 15 min treatment time is how long the sample was held at the highest temperature, pyrolysis reactions will also take place during the heating and cooling phases. Benchmarking experiments were also conducted with pyrene-contaminated soil (43% clay; 7 ppm iron content) to illustrate the beneficial catalytic effect of ion-exchanged clays. These experiments were carried out only at 150 °C with 15 min treatment time.

Analysis of Solvent-Extractable Compounds and Pyrene Measurement. We analyzed the acetone-extractable hydrocarbons and residual pyrene concentrations of pyrolyzed samples via gas chromatography and mass spectrometry (GC−MS) and UV−visible spectrophotometry (UV−Vis). Using an extraction method modified from a previous study,[24] 100 mg of pyrolyzed sample was placed in a centrifuge tube with 2 mL of acetone. The mixture was extracted in an ultrasonic bath for 30 min and centrifuged at 10,000 rpm for 10 min. The supernatants were then filtered through a 0.2 μm membrane filter, placed in 2 mL GCMS vials, and stored in a 4 °C refrigerator until analysis.

Pyrene was quantified, and the intermediate products were identified using a gas chromatograph (Agilent 7820A) equipped with a mass spectrum detector (Agilent 5977E) using EPA Method 8275A (LOD ~5 mg/kg). A HP-5ms Ultra Inert capillary column (30 m × 0.25 mm × 0.25 μm film thickness) (Agilent Technologies) was used. The flow rate of helium carrier gas was kept at 1 mL/min with splitless injection at an inlet temperature of 275 °C. The initial column temperature was 80 °C and held for 1 min before ramping at 25 °C/min to 200 °C and then increased to 256 °C at the rate of 8 °C/min and held for 5 min. Pyrene was quantified using the selected ion monitoring (SIM) mode with target ions (m/z) of 202 and 101. The decomposition products were acquired in full scan mode from m/z 29 to 350 with an acquisition frequency of 4.4 scans per second. Pyrene decomposition products were also analyzed with a UV−Vis spectrophotometer (NanoDrop One Microvolume) by obtaining spectra from 190 to 900 nm, which is the characteristic absorbance range of aromatic compounds.[25]

MTT Assay of Cell Viability. A colorimetric cell viability assay with human bronchial epithelial cells was used to determine the toxicity of samples treated at different pyrolysis temperatures.[7] For these tests, we used BEAS-2B normal human bronchial epithelial cells infected with a replication-defective SV40/adenovirus 12 (ATCC # CRL-9609), an MTT Cell Proliferation Assay Kit (ATCC # 30-1010K), and RPMI 1640 medium (Sigma-Aldrich). After extracting the pyrolysis products from the treated solids with acetone, 0.5 mL from each extract was evaporated at room temperature in a fume hood and reconstituted in 100 μL of DMSO (Sigma-Aldrich). The MTT assay was performed in 96-well plates. First, 2000 cells in 100 μL of culture medium were placed in each well and kept overnight. Next, 1 μL of 1:2.5 diluted extract sample (or 1 μL of DMSO control) was added into each well and incubated for 24 h. After incubation, 10 μL of MTT reagent was added to each well and incubated again for 2 h until a purple precipitate was visible. Finally, 100 μL of detergent reagent was added and left at room temperature in the dark for 2 h. A fluorescence plate reader (SpectraMax GeminiXS) was used to determine cell viability by measuring the absorbance at 570 nm.

DFT Method. All density functional theory (DFT) calculations were carried out using the Vienna ab initio simulation package (VASP 5.4.4).[26] The exchange correlation functional was the Perdew−Burke−Ernzerhof (PBE)[27] implementation of the generalized gradient approximation (GGA). The projector-augmented wave (PAW) method[28] was employed with VASP default potentials[29] to treat frozen-core electrons. The self-consistent-field (SCF) optimization of the electronic structure treated the following valence electrons explicitly: Fe($3d^64s^2$), Mg($3s^2$), Al($3s^23p^1$), Si($3s^23p^2$), C-($2s^22p^2$), H($1s^1$), O($2S^22P^4$), Cu($3d^{10}4s^1$), Na($2p^63s^1$), and Zn($3d^{10}4s^2$). The plane-wave basis set cutoff energy was 500 eV. The Gaussian smearing method was applied with a smearing width of 0.05 eV. Brillouin zone integration was conducted with the Monkhorst−Pack scheme with a 3 × 3×1 k-point grid.[30] The DFT-D3 method of Grimme[31] was employed in all calculations to treat van der Waals interactions. The total energy during SCF cycles was converged to $<10^{-5}$ eV, and geometries were optimized by minimizing the forces to <0.02 eV Å^{-1}. All calculations were spin-polarized.

Modeling the amorphous phase of soil is a very challenging task, given the presence of numerous unknown elements and the high complexity of the system. However, we can use DFT to determine the relative reactivity of individual sites by modeling them one at a time. Thus, we applied DFT to investigate the reducibility of well-defined catalytic sites that are likely present on the bentonite surfaces. As such, we constructed slab models with the stoichiometry adjusted to create model sites with known formal oxidation states (i.e., Fe^{3+}, Fe^{2+}, Cu^{2+}, Cu^{+}, Zn^{2+}, and Na^{+}). We find that the oxidation state of the transition metal cation site plays a key role because it determines the reducibility of the site and thus its catalytic activity toward hydrocarbons.

We modeled the bentonite surface by cleaving a (001) facet from a geometry-optimized Montmorillonite (the main component of bentonite) bulk structure (Figure S1).[32] The simulation cell had dimensions of 10.36 Å × 8.98 Å × 30 Å, which created a separation of approximately 20 Å between slab layers. The stoichiometry of the "pure" bentonite surface model was Si_2AlO_6H, yielding formal oxidation states of Si^{4+}, Al^{3+}, O^{2-}, and H^{+}. Ion-exchanged adsorption site models with surface Fe, Cu, Zn, or Na cations were generated by placing one cation on a surface hollow site (Figure S2).

XPS analysis of untreated and uncontaminated Fe-bentonite and Cu-bentonite after ion-exchange was conducted to determine the surface oxidation state of the metal (Figure S3). Fe-bentonite shows a predominant oxidation state of Fe^{3+} at 711.5 eV,[33] and Cu-bentonite exhibits a primary oxidation state of Cu^{2+}.[34,35] Models with surface and sub-surface transition metals yield similar conclusions (see Supporting Information Text S2). The impregnation method is unlikely to induce the creation of Al/Si vacancies that could be filled with the transition metal cations to form anti-site defects, since the measured compositions (Table 1) show that the amount of Si and Al did not change after the ion-exchange.

The impregnation method is unlikely to induce the creation of Al/Si vacancies that could be filled with the transition metal cations to form anti-site defects since the measured compositions (Table 1) show that the amount of Si and Al did not change after the ion-exchange. Thus, we chose to model the transition metal cation adsorbed on the surface as shown in Figure S2.

We adjusted the stoichiometry of the slab model to achieve the desired oxidation states for the cations. Substituting a neutral atom with a neutral atom of a different identity with one fewer valence electron creates an electron deficiency on the surface. The formal oxidation state of the adsorbed transition metal can be controlled by introducing these substitutions as the adsorbed metal supplies electrons to remove the electron deficiency. A model with two Mg-for-Al (Mg_{Al}) substitutions and one Al-for-Si (Al_{Si}) substitution was used for Fe^{3+}, a model with two Mg_{Al} substitutions was used for Cu^{2+} and Zn^{2+}, and a model with one Mg_{Al} substitution was used for Na^{+}.

The adsorption energy (E_{ads}) of the pyrene molecule on the various cation sites was calculated according to eq 1

$$E_{ads} = E_{surf\_molecule} - E_{molecule} - E_{surf} \tag{1}$$

where $E_{surf\text{-}molecule}$ represents the total energy of the bentonite surface with the adsorbed pyrene molecule, $E_{molecule}$ represents the energy of an isolated pyrene molecule placed in a 20 × 20 × 20 Å3 simulation cell, and E_{surf} represents the energy of the bentonite surface. A more negative energy value indicates a stronger binding interaction between pyrene and the surface. The adsorption energy of a hydrogen atom (E_{H_ads}) on different sites with various cations (Figure S4) was calculated according to eq 2

$$E_{H\_ads} = E_{surf\text{-}H} - {}^{1}\!/_{2}E_{H_2} - E_{surf} \tag{2}$$

where $E_{surf\text{-}H}$ represents the total energy of the surface with an adsorbed hydrogen atom, E_{H_2} represents the energy of an isolated hydrogen molecule placed in a 15 × 15 × 15 Å3 simulation cell, and E_{surf} represents the energy of the surface without the adsorbed hydrogen atom. A more negative energy value indicates a stronger binding interaction between the hydrogen atom and the surface, which indicates greater site reducibility. All possible hydrogen binding sites on the surface were tested to determine the most favorable hydrogen binding site (see Figure S4 for site definitions).

Data Analysis. All TGA pyrolysis experiments were run in triplicates. Residual pyrene concentrations were determined from at least three pyrolyzed samples at 150, 200, or 300 °C, and averages with standard errors were calculated. Statistical significance of differences was assessed using Student's *t*-test at the 95% confidence level.

RESULTS AND DISCUSSION

Pyrene Removal Efficiency Depends on the Type of Ion-Exchanged Transition Metal Used. PAHs adsorb strongly on metal sites of clays via cation−π interactions.[36−38] These interactions could promote the formation of environmental-persistent free radicals (EPFRs)[39] or trigger oligomerization reactions that form higher molecular weight aromatic species.[40] To further explore the catalytic role of clay transition metals on PAH degradation, we studied the pyrolytic degradation of pyrene deposited on pure or metal-impregnated bentonite.

For the first set of experiments, pyrene-spiked samples were pyrolyzed for 15 min at 300 °C, the lowest temperature used in our previous study.[18] For natural bentonite, the pyrene concentration decreased from 1000 to 371 mg/kg for a removal efficiency of 63% (Table 2). The removal efficiency was significantly higher for ion-exchanged Fe-bentonite (∼100%), Cu-bentonite (97%), and Zn-bentonite (81%) with residual pyrene concentrations of less than 5, 31, and 189 mg/kg, respectively. Thus, ion-exchanged transition metals significantly enhance pyrene degradation.

Table 2. Residual Pyrene Concentrations (mg/kg) and Removal Efficiency (in Parentheses) for Pyrolysis Experiments at 150, 200, and 300 °C with a 15 min Treatment Time of Pyrene-Contaminated Bentonite, Fe-Bentonite, Cu-Bentonite, and Zn-Bentonite

	300 °C for 15 min	200 °C for 15 min	150 °C for 15 min
Pure Bentonite	371 ± 66 (63%)	529 ± 47 (47%)	519 ± 99 (48%)
Fe-Bentonite	<5 (∼100%)	9 ± 2 (99%)	67 ± 48 (93%)
Cu-Bentonite	31 ± 23 (97%)	88 ± 29 (91%)	285 ± 57 (72%)
Zn-Bentonite	189 ± 108 (81%)	456 ± 34 (55%)	570 ± 109 (43%)

At 200 °C and 15 min treatment time, the pyrene concentration in natural bentonite decreased from 1000 to 529 mg/kg (47% removal efficiency). For the same conditions, both Fe-bentonite and Cu-bentonite again exhibited higher removal efficiencies (99% and 91%, respectively), with respective residual pyrene concentrations of 9 and 88 mg/kg (Table 2). Zn-bentonite, on the other hand, exhibited lower pyrene removal efficiency (55%) with a residual pyrene concentration of 456 mg/kg (Table 2). However, all three ion-exchanged clays achieved higher conversion of pyrene than the natural bentonite at temperatures from 200 to 300 °C.

The high pyrene removal levels achieved by Fe- and Cu-bentonite at 200 °C prompted us to carry out additional experiments at the unprecedentedly low pyrolysis temperature of 150 °C with 15 min treatment time (Figure 1). Natural bentonite contains iron and other cations (Table 1) and exhibited a significantly higher pyrene removal efficiency (48%) than that of the control soil (4%), with 43% clay content (Figure 1). Zn enrichment did not significantly enhance pyrene removal (Figure 1). On the other hand, Fe-bentonite and Cu-bentonite again exhibited high pyrene removal efficiencies of 93% and 72%, respectively. These results suggest that PAH sorption to transition metals in clays is important to promote PAH degradation, and sorption affinity varies widely with the amount and type of the cations they contain. The importance of pyrene sorption for pyrocatalytic degradation was illustrated in control experiments using pyrene deposited on pure quartz samples, which did not

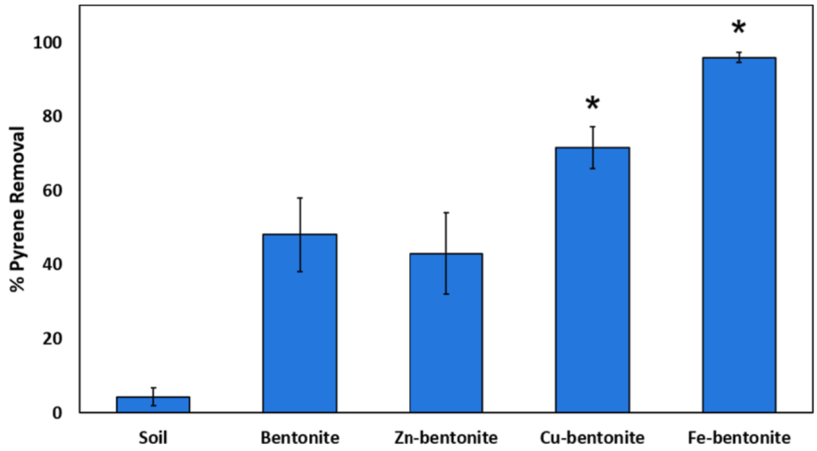

Figure 1. Enhanced pyrene removal by bentonite and bentonite enriched with ion-exchanged transition metals at unprecedentedly low pyrolysis temperature of 150 °C with a 15 min treatment time. Initial pyrene concentration was 1000 mg/kg. Data show the mean ± the standard deviation. Asterisks (*) denote significantly higher removal than for baseline bentonite at the 95% confidence level.

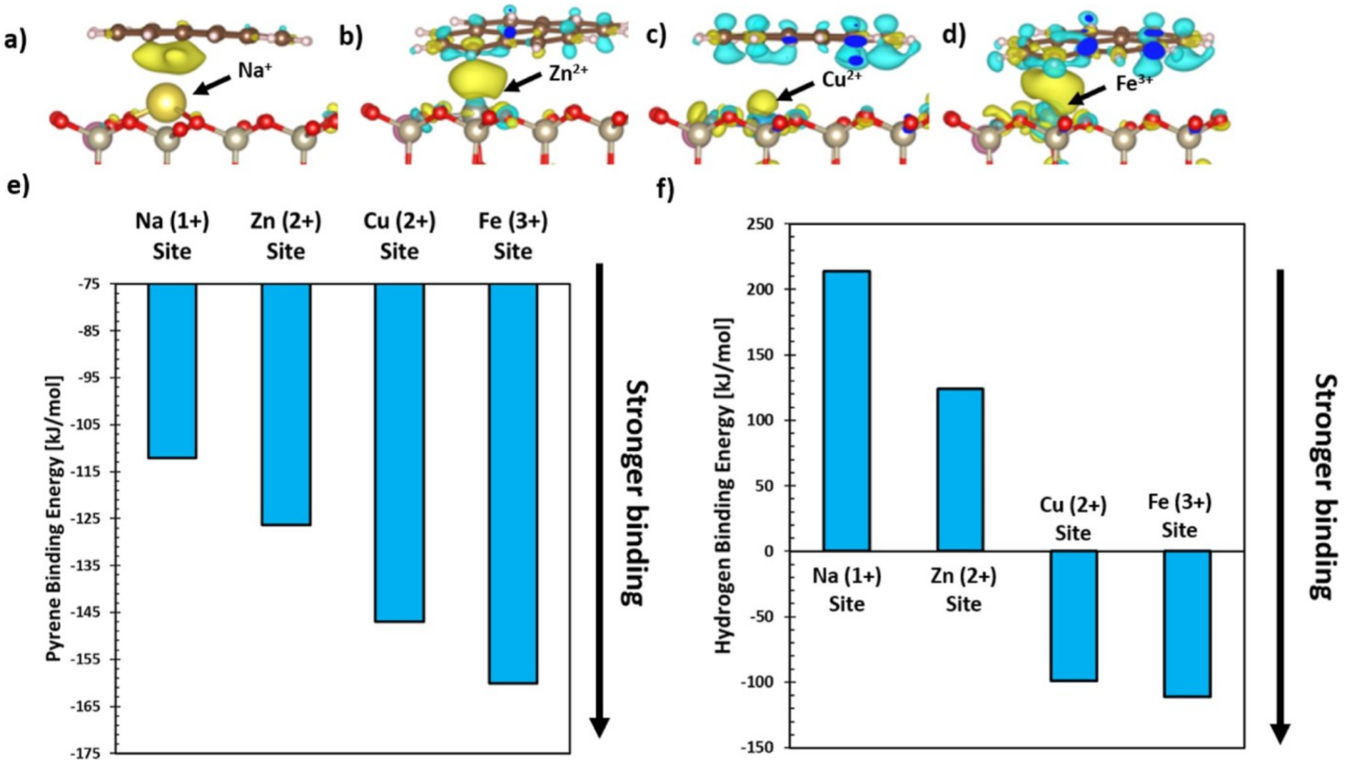

Figure 2. DFT-calculated charge density difference plots for pyrene absorption on the (a) Na^+ site, (b) Zn^{2+} site, (c) Cu^{2+} site, and (d) Fe^{3+} site. Yellow and cyan isosurfaces (0.0017 e− $Å^{-3}$) represent electron accumulation and depletion, respectively. (e) Pyrene adsorption energies on the different cation sites. (f) Hydrogen atom adsorption energies on the most favorable site (see Figure S4 and Table S3 for all site definitions and adsorption energies) for different cations. Charge density difference plots for hydrogen adsorption are shown in Figure S6.

yield degradation products or char. Instead, the deposited pyrene devolatilized and/or sublimated at temperatures between 100 and 200 °C (Figure S5).

In general, the beneficial effect of Fe and Cu in bentonite was significantly higher than that of Zn at all tested temperatures. The high removal efficiency of pyrene with Fe and Cu at 150 °C highlights the potential of these earth-abundant metals for enhancing pyrolytic treatment. Pyrolysis at such low temperatures would allow us to meet regulatory requirements with significantly lower energy requirements and operating costs.

While our results demonstrate that pyrene degradation is catalyzed by transition metals, the catalytic activity and, thus, the overall conversion efficiency of a metal depend on several factors such as its ionization potential,[24,39,41] polarizability,[37] and where the metal is located in the clay structure.[24,37,39,42,43] Surface area can also affect the adsorption of PAHs and subsequent catalytic reactions.[44] The bentonite BET surface area increased from about 35 to 42−46 m^2/g after transition metal amendment via ion exchange. Liquid-phase ion-exchange with transition metals can modify bentonite interlayer spacing and pore distribution, leading to increased surface area.[45,46] However, the BET method does not measure the active surface

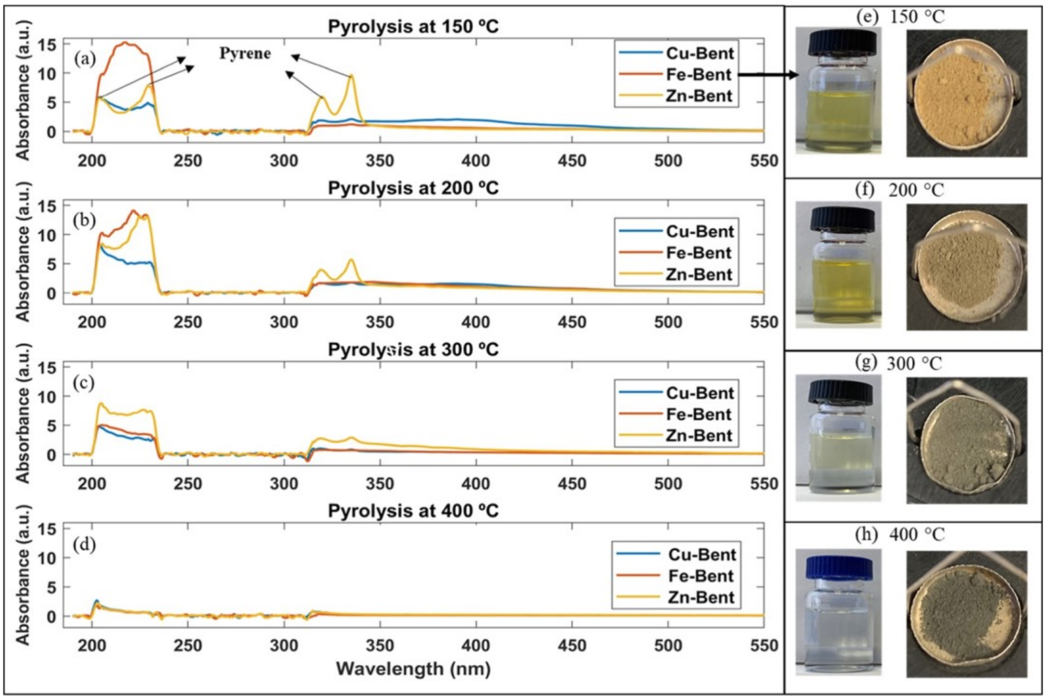

Figure 3. UV−Vis spectra of extracts from ion-exchanged Fe, Cu, and Zn bentonites pyrolyzed at (a) 150, (b) 200, (c) 300, and (d) 400 °C with a 15 min contact time. Residual pyrene (see peaks located at 204, 230, 319, and 335 nm) and decomposition products were detected in the extracts for pyrolysis temperatures below 400 °C. Panels (e−h) show images of Fe-bentonite extracts and solid samples treated at the indicated temperatures. The color of the extracts indicates that they contain varying concentrations of pyrene decomposition products absorbing in the visible range (380−550 nm), while the progressively darker color of the solid residues indicates the formation of char as the pyrolysis temperature increases.

area where the catalytic reaction is taking place. Moreover, the relatively small differences in the BET surface areas of the three bentonites amended with Fe, Cu, or Zn cannot account for their widely different reactivities. As discussed below, several additional factors may determine the strength of the π-cation bond between a PAH molecule and a cationic metal site, as well as the mechanism and extent to which they catalyze PAH transformations during thermal treatment.

Pyrene Absorption on Bentonite Surfaces. We applied DFT to compute the binding energy of pyrene on different cation sites (defined by eq 1). These calculations allow us to assess the strength of the pyrene adhesion on different surface sites, as well as the extent of charge transfer between pyrene and the surface cation (Figure 2). The computed adsorption energies of pyrene on bentonite surfaces are −84 kJ/mol on the stoichiometric surface with no adsorbed cation, −112 kJ/mol on the Na^+ site, −126 kJ/mol on the Zn^{2+} site, −147 kJ/mol on the Cu^{2+} site, −98 kJ/mol on the Cu^+ site, −160 kJ/mol on the Fe^{3+} site, and −114 kJ/mol on the Fe^{2+} site. We also applied DFT to compute the hydrogen atom adsorption energies on different cation sites (defined by eq 2) to quantitatively assess the reducibility of the different transition metal cation sites. Previous literature[47−49] has established hydrogen adsorption energy as a direct descriptor of site reducibility, as well as showed that it is a good predictor of hydrocarbon activation rates over oxide-based catalysts. The hydrogen adsorption energies on different cation sites are reported in Table S2, where a lower energy value indicates stronger binding, signifying that hydrogen tends to adsorb on the surface, thereby indicating greater surface site reducibility. The associated charge density difference plots for hydrogen binding clearly show that the metal cation acts as the reduction center (Figure S6).

The nature of charge transfer from the pyrene molecule as well as from the hydrogen atom to the adsorption site is visualized in Figures 2a−d and S6 by subtracting the optimized electron density of the entire adsorbate + surface system from that of the isolated surface and adsorbate ($\rho_{\text{diff}} = \rho_{\text{surf+adsorbate}} - \rho_{\text{adsorbate}} - \rho_{\text{surf}}$). The resulting isostructural charge density difference represents the redistribution of charge as the pyrene molecule or a hydrogen atom adsorbs on the surface. Note that the appearance of the isosurfaces is significantly influenced by the shape and size of the molecular orbitals involved in the charge transfer process. As such, the visual size of the charge density difference isosurfaces in Figure 2a−d as well as in Figure S6 does not quantitatively indicate the amount of charge transferred or the associated change in energy. Visualization of the isosurfaces is useful to reveal the regions where the electron density redistributes during the interaction between adsorbate and cations. Therefore, the isosurfaces in Figures 2a−d and S6 should only be interpreted qualitatively to understand the nature of the charge transfer, such as the origin (the HOMO of pyrene) and destination (the cation) of the charge (Figure S7). The isosurfaces shown in Figures 2 and S6 demonstrate that the cation site serves as the reduction center.

Based on the computed pyrene binding (Figure 2e) and hydrogen adsorption strength on various cation sites (Figure 2f), we observe stronger binding with pyrene and hydrogen on Fe^{3+} and Cu^{2+} sites compared to the Na^+ and Zn^{2+} sites, which is intuitive based on the available oxidation states of the cations. The reduction of Fe^{3+} to Fe^{2+} or Cu^{2+} to Cu^+ is energetically favorable, whereas reduction of Zn^{2+} to Zn^+ or

Na^+ to Na^0 is unfavorable. We also tested the pyrene and hydrogen binding on Fe^{2+} and Cu^+ sites, which were unfavorable because Fe^{2+} to Fe^+ and Cu^+ to Cu^0 reductions are unfavorable (Figures S8 and S9 and Table S3). Hence, we expect that the Fe^{3+} and Cu^{2+} sites exhibit stronger catalytic effects compared to Na^+, Zn^{2+}, Cu^+, and Fe^{2+} sites.

We posit that the Fe and Cu ion-exchanged bentonites contain more reducible sites that can oxidize pyrene, which in turn promotes pyrolysis at lower temperatures. The ion-exchanged samples shown in Figure 1 have many different types of sites, as is evident from the compositions in Table 1. For example, Zn-bentonite and Cu-bentonite both still have significant Fe content. As such, we cannot draw a one-to-one comparison between the measured extent of pyrene removal shown in Figure 1 and the binding strengths computed in Figure 2. Such a comparison would require us to know exactly how many active sites of each cation type are in each sample, which is complicated by the fact that not all cations can be assumed to reside in the same type of site. For example, some Fe sites might be more active on how the cation is bound to the surface. However, the DFT results do indicate that pyrene adsorption is enhanced on cation sites that can accommodate an electron transfer from the HOMO of pyrene (such as $Fe^{3+} \rightarrow Fe^{2+}$ or $Cu^{2+} \rightarrow Cu^+$). Upon examining the computed hydrogen adsorption energies on various cation sites, a clear trend is that Fe^{3+} and Cu^{2+} sites are more active than Zn^{2+} and Na^+ sites (Figure 2f), indicating that these former sites are highly reducible and can receive an electron during pyrene activation as the metal cations clearly serve as the reduction center (Figure S6).

Pyrene Decomposition Products Depend Both on the Dominant Transition Metal and the Pyrolysis Temperature. To further investigate the effect of temperature and enriched transition metal on pyrene degradation, we used UV−Vis spectroscopy to measure the absorbance of the extracts from pyrene-spiked samples pyrolyzed at different temperatures (Table 2 and Figure 3). The extracts from Fe-bentonite samples pyrolyzed at 150 and 200 °C had a dark yellow color but progressively became colorless as the temperature increased to 400 °C (Figure 3e−h). Similar color changes with pyrolysis temperatures were observed for the extracts from the other samples (Figure S10). In a previous study, we also observed that heavy diesel fuels changed from colorless to yellow due to the formation of polymerization products catalyzed by Cu−Y zeolites.[50,51]

GC−MS spectroscopy was also used to analyze the acetone extracts from all pyrolyzed solids. Extracts from pyrene-spiked Fe-bentonite samples pyrolyzed at temperatures between 150 and 300 °C contained several single-ring aromatics (arenes), methylated acetophenones, and naphthalene (Table S4). Oxygenated compounds detected in the extracts may be due to reactions between pyrene degradation products with the water present in bentonite. This observation is consistent with previous studies that observed the formation of oxygenated compounds during the thermal decomposition of pyrene in air and water with redox-active materials.[12] In contrast, almost no products were detected at 400 °C, except for 1,3-bis(1,1-dimethylethyl)-benzene, which was also present in the original bentonite extract and was not a product of pyrene decomposition (Table S4). Extracts from the pyrene-spiked bentonite, Cu-bentonite, and Zn-bentonite samples contained significant amounts of unreacted pyrene and had to be diluted for GC−MS analysis. As a result, pyrene degradation products could not be easily detected on the GC−MS spectra for these extracts.

The distribution of solvent-extracted degradation products was affected by both the pyrolysis temperature and the dominant transition metal (Figure 3a−d). To interpret this figure, note that small aromatics (e.g., arenes and naphthalene) absorb in the UV range (<380 nm) (Figure S11), while high-molecular-weight hydrocarbons like PAHs or oxidized PAHs absorb mostly in the visible range (>380 nm).[52] Pyrene in acetone exhibits two sharp double peaks at 204 and 230 nm and again at 319 and 335 nm (Figure S12). The gap between 235 and 313 nm is due to acetone that absorbs very strongly in this range (Figure S13) and wipes out the absorbance of pyrene degradation products that are present in very small concentrations.

At 150 °C, the UV−Vis spectrum of Fe-bentonite extract exhibits a strong absorbance peak between 200 and 235 nm due to small aromatics (Table S4). The Cu-bentonite extract has a much smaller peak in the 200−235 range, indicating that Cu formed fewer small aromatics than Fe at this temperature because its pyrene conversion is lower (Table 2). However, Cu-bentonite has a broad peak in the visible range between 350 and 450 nm, which can be attributed to larger aromatic byproducts.[53] High-molecular-weight degradation products absorb in the 310−550 range and give the yellow color to the extracts (Figure 3e). The Zn-bentonite data show that significant amounts of unreacted pyrene remain at 150 °C, as indicated by the double peaks at 319 and 335 nm. Unreacted pyrene also contributes to the absorbance in the 200−235 nm range (Figure 3a).

At 200 °C, Fe-bentonite produces fewer small aromatics and more large aromatics than at 150 °C. On the other hand, Cu-bentonite produces more small aromatics and fewer large aromatics than at 150 °C. When the temperature increases to 300 °C, however, the amounts of both the small and the large aromatic products for Fe and Cu become about equal and decrease even more until they almost completely disappear for 400 °C, where the final degradation product is primarily char. Similar trends were observed for Zn-bentonite whose spectra indicate unreacted pyrene at 300 °C, but a near-complete conversion of pyrene to char at 400 °C.

In summary, pyrene pyrolysis at 150 and 200 °C yielded acetone-extractable products, with the ratio of small to large aromatics depending on the dominant transition metal and associated pyrene conversion efficiency. When the pyrolysis temperature increased to 300 °C, the product distribution shifted from extractable degradation products to char. Very small amounts of extractable products were detected at 400 °C, and char was the main pyrolysis product at this temperature.

High Temperatures Favor Char Formation over Extractable Decomposition Products. Pyrolytic treatment converts aromatic hydrocarbons to char, a stable and nontoxic end product, via radical polymerization reactions.[5,54−61] We previously showed that the pyrolysis of crude-oil contaminated soils generates a thin film of coke on the soil particles.[6] This was confirmed by elemental analysis and X-ray photoelectron spectroscopy experiments detecting higher amounts of carbon on the surface of the soil.[5,6] Partial combustion experiments also confirmed the presence of char by detecting higher amounts of CO_2 in the outlet gas stream when the treated sample was exposed to oxygen.[5]

Figure 3 shows that increasing pyrolysis temperatures result in a progressively darker color indicative of char formation.

https://doi.org/10.1021/acs.est.3c04487

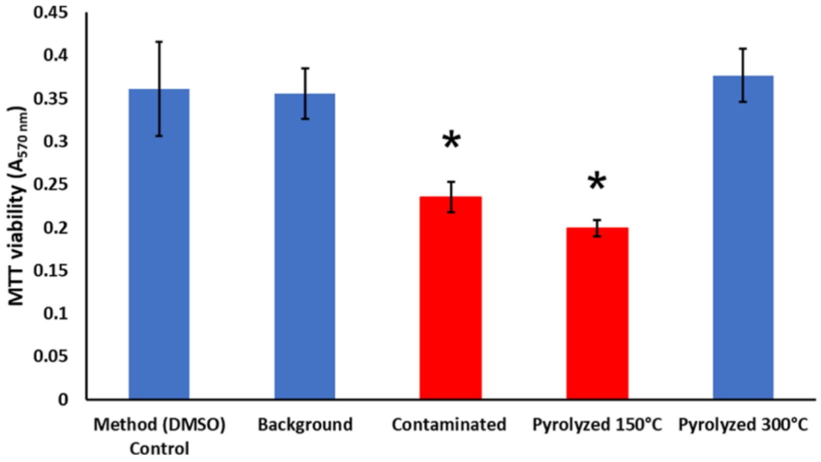

Figure 4. MTT viability assays show that pyrolytic treatment at low temperatures (150 °C) does not remove residual toxicity for Fe-bentonite despite high pyrene removal efficiency. The background or negative control was Fe-bentonite without pyrene, and the contaminated or positive control was untreated Fe-bentonite that contained 1000 mg/kg of pyrene. The method control was DMSO without any acetone extract. Error bars represent plus or minus one standard deviation from the mean. Asterisks (*) denote significantly higher residual toxicity compared to the DMSO experimental control at the 95% confidence level.

These visual observations and the fact that the 400 °C extracts contain almost no pyrene degradation products (Figure 3d) infer that pyrene is converted to char at this temperature, which is consistent with the observed detoxification (Figure 4). XPS analysis corroborated the presence of char on the surface of pyrolyzed Fe-bentonite at 400 °C (Text S1), which was removed when this pyrolyzed Fe-bentonite was reacted in the TGA with a 60/40 oxygen/nitrogen mixture at 550 °C. These results agree with previous work[5] showing that char formation increases with increasing pyrolysis temperatures. Similar color changes with increasing pyrolysis temperature are observed for all pyrolyzed samples (Figure S14). Thus, all tested transition metal catalysts favor the formation of char at higher temperatures.

Trade-Offs between Pyrolysis Temperature and Residual Toxicity. The positive control for our toxicity study was pyrene-spiked but untreated Fe-bentonite whose extract, as expected, exhibited significant toxicity (Figure 4). Although high pyrene removal efficiency (>93%) was observed for Fe-bentonite at only 150 °C with 15 min contact time (Figure 1), the treated solid residue had significantly higher residual toxicity to lung cells (i.e., lower cell viability) than either the uncontaminated Fe-bentonite (negative control) or the DMSO method control (Figure 4). This is probably because pyrolysis at this low temperature produced toxic degradation products (Figure 3, Table S4). Moreover, the extract from pyrene-spiked Fe-bentonite treated at 150 °C exerted oxidative stress in cells (Figure S15).[62] These observations demonstrate that low pyrolysis temperatures may achieve regulatory cleanup standards but do not guarantee detoxification.

However, pyrolytic treatment of pyrene-contaminated Fe-bentonite at 300 °C for 15 min eliminated the toxicity of the solid residue, which had similar lung cell metabolic activity to that of the negative control. Treatment at 300 °C seems to completely detoxify the contaminated bentonite even though some (apparently less toxic) PAH byproducts (e.g., ethanone fragments and straight chain hydrocarbons) were detected in the extracts (Table S4).

ENVIRONMENTAL IMPLICATIONS

Overall, this work shows that high pyrene removal efficiency can be achieved at unprecedentedly low pyrolytic treatment temperatures (e.g., 150 °C) with clays impregnated with earth-abundant transition metals. The high removal efficiency can be explained by DFT calculations, which showed that pyrene adsorbs strongly on clays containing Fe^{3+} or Cu^{2+} sites that can accommodate an electron transfer from the HOMO of pyrene. Fe^{3+} and Cu^{2+} are effective at capturing pyrene and facilitating an electron transfer that leads to the formation of unstable radicals. We also observed the formation of char, a stable and acceptable end-product, from the pyrolysis of pyrene, which has not been previously demonstrated.

Lower pyrolytic treatment temperatures decrease both energy requirements and contact times needed to meet regulatory cleanup standards, resulting in lower operating costs, higher throughput capacity, and a smaller carbon footprint. Thus, the presence of clay-embedded transition metals (or their amendment) would enhance the feasibility and applicability of large-scale pyrolytic soil remediation. However, the energy-savings, higher treatment capacity, and other potential benefits associated with such amendments (e.g., improved fertility of treated soils) would need to be evaluated against potential costs (including additional disposal burden), as part of techno-economic analyses that are generally conducted at later stages of technology development.

Our results infer that high PAH removal efficiency does not guarantee full detoxification of contaminated soil, and mitigating the formation of byproducts that contribute to residual toxicity may require higher pyrolysis temperatures. Thus, managing such trade-offs between pyrolysis temperature and residual toxicity requires careful consideration of how soil components and contaminant characteristics influence the kinetics and pyrolysis reaction pathways. Improved predictive understanding of such interactions should guide safe application and inform process optimization models.

ASSOCIATED CONTENT

Supporting Information

The Supporting Information is available free of charge at https://pubs.acs.org/doi/10.1021/acs.est.3c04487.

DFT surface models; XPS elemental scans; additional XPS methods; DFT top-down view of hydrogen adsorption sites; weight loss of sand contaminated with pyrene during pyrolysis; DFT-calculated hydrogen adsorption energies on Na^+, Zn^{2+}, Cu^{2+}, and Fe^{3+}; DFT charge density difference plots; HOMO of pyrene and charge differences on transition metal sites; DFT-calculated charge density difference plots for pyrene adsorption on Cu^+ and Fe^{2+} sites; DFT-calculated charge density difference plots for hydrogen atom adsorption on Cu^+ and Fe^{2+} sites; DFT-calculated hydrogen adsorption energies on Cu^{2+}, Cu^+, Fe^{3+}, and Fe^{2+}; extract images after pyrolysis treatment; compounds detected on the GCMS after treatment; UV−Vis spectrum of a hydrocarbon mixture, pyrene, and acetone; char images after pyrolysis treatment; and H_2O_2 ROS generation of pyrene-spiked Fe-bentonite after treatment at 150 and 300 °C (PDF)

AUTHOR INFORMATION

Corresponding Authors

Kyriacos Zygourakis − *Department of Chemical and Biomolecular Engineering, Rice University, Houston, Texas 77005, United States;* orcid.org/0000-0002-1044-1139; Email: kyzy@rice.edu

Pedro J. J. Alvarez − *Department of Civil and Environmental Engineering, Rice University, Houston, Texas 77005, United States;* orcid.org/0000-0002-6725-7199; Email: alvarez@rice.edu

Authors

Sara B. Denison − *Department of Civil and Environmental Engineering, Rice University, Houston, Texas 77005, United States*

Peixuan Jin − *Department of Chemical and Biomolecular Engineering, Rice University, Houston, Texas 77005, United States*

Priscilla Dias Da Silva − *Department of Chemical and Biomolecular Engineering, Rice University, Houston, Texas 77005, United States*

Chun Chu − *Neonatology Research Program, Department of Pediatrics, Baylor College of Medicine, Houston, Texas 77030, United States*

Bhagavatula Moorthy − *Neonatology Research Program, Department of Pediatrics, Baylor College of Medicine, Houston, Texas 77030, United States*

Thomas P. Senftle − *Department of Chemical and Biomolecular Engineering, Rice University, Houston, Texas 77005, United States*

Complete contact information is available at:
https://pubs.acs.org/10.1021/acs.est.3c04487

Notes

The authors declare no competing financial interest.

ACKNOWLEDGMENTS

Research reported in this publication was supported by the National Institute of Environmental Health Sciences of the National Institutes of Health [Grant Number P42ES027725]. The content is solely the responsibility of the authors and does not necessarily represent the official views of the National Institutes of Health. P.J. and T.P.S. acknowledge partial funding support from the National Science Foundation (Awards # CBET-2143941 and EEC-1449500).

REFERENCES

(1) Hussain, K.; Hoque, R. R.; Balachandran, S.; Medhi, S.; Idris, M. G.; Rahman, M.; Hussain, F. L. Monitoring and Risk Analysis of PAHs in the Environment. In *Handbook of Environmental Materials Management*; Hussain, C. M., Ed.; Springer International Publishing: Cham, 2018; pp 1−35. DOI: DOI: 10.1007/978-3-319-58538-3_29-2.

(2) Kang, C. U.; Kim, D. H.; Khan, M. A.; Kumar, R.; Ji, S. E.; Choi, K. W.; Paeng, K. J.; Park, S.; Jeon, B. H. Pyrolytic Remediation of Crude Oil-Contaminated Soil. *Sci. Total Environ.* 2020, *713*, 136498.

(3) Suter, M. A.; Aagaard, K. M.; Coarfa, C.; Robertson, M.; Zhou, G.; Jackson, B. P.; Thompson, D.; Putluri, V.; Putluri, N.; Hagan, J.; Wang, L.; Jiang, W.; Lingappan, K.; Moorthy, B. Association between Elevated Placental Polycyclic Aromatic Hydrocarbons (PAHs) and PAH-DNA Adducts from Superfund Sites in Harris County, and Increased Risk of Preterm Birth (PTB). *Biochem. Biophys. Res. Commun.* 2019, *516*, 344−349.

(4) Li, F.; Su, Q.; Zhou, Z.; Liao, X.; Zou, J.; Yuan, B.; Sun, W. Anaerobic Biodegradation of 8:2 Fluorotelomer Alcohol in Anaerobic Activated Sludge: Metabolic Products and Pathways. *Chemosphere* 2018, *200*, 124−132.

(5) Vidonish, J. E.; Alvarez, P. J. J.; Zygourakis, K. Pyrolytic Remediation of Oil-Contaminated Soils: Reaction Mechanisms, Soil Changes, and Implications for Treated Soil Fertility. *Ind. Eng. Chem. Res.* 2018, *57*, 3489−3500.

(6) Vidonish, J. E.; Zygourakis, K.; Masiello, C. A.; Gao, X.; Mathieu, J.; Alvarez, P. J. Pyrolytic Treatment and Fertility Enhancement of Soils Contaminated with Heavy Hydrocarbons. *Environ. Sci. Technol.* 2016a, *50*, 2498−2506.

(7) Song, W.; Vidonish, J. E.; Kamath, R.; Yu, P.; Chu, C.; Moorthy, B.; Gao, B.; Zygourakis, K.; Alvarez, P. J. J. Pilot-Scale Pyrolytic Remediation of Crude-Oil-Contaminated Soil in a Continuously-Fed Reactor: Treatment Intensity Trade-Offs. *Environ. Sci. Technol.* 2019, *53*, 2045−2053.

(8) Liu, Y. Q.; Zhang, Q.; Wu, B.; Li, X. D.; Ma, F. J.; Li, F. S.; Gu, Q. B. Hematite-Facilitated Pyrolysis: An Innovative Method for Remediating Soils Contaminated with Heavy Hydrocarbons. *J. Hazard. Mater.* 2020, *383*, 121165.

(9) Liu, Y.; Li, X.; Zhang, W.; Dou, J.; Zhang, Q.; Ma, F.; Gu, Q. Effect and Mechanisms of Red Mud Catalyst on Pyrolysis Remediation of Heavy Hydrocarbons in Weathered Petroleum-Contaminated Soil. *J. Environ. Chem. Eng.* 2021, *9*, 106090.

(10) Liu, Y.; Li, X.; Zhang, W.; Ma, F.; Zhang, Q.; Gu, Q. Pyrolysis of Heavy Hydrocarbons in Weathered Petroleum-Contaminated Soil Enhanced with Inexpensive Additives at Low Temperatures. *J. Cleaner Prod.* 2021, *302*, 127017.

(11) Lin, F.; Yu, H.; Li, J.; Zygourakis, K.; Li, R.; Cheng, Z.; Yan, B.; Chen, G. Investigation on the Interaction between Oil Compositions and Soil Minerals with the Targets of Resource Recovery and Harmless Disposal of Oily Sludges by Pyrolysis. *ACS ES&T Engg* 2023, *3*, 734−744.

(12) Oden, C. P.; Werth, C. J.; Notini, L.; Katz, L. E. Fate of Pyrene on Mineral Surfaces during Thermal Remediation as a Function of Temperature. *Environ. Sci.: Processes Impacts* 2022, *24*, 1181−1194.

(13) Li, J.; Lin, F.; Yu, H.; Tong, X.; Cheng, Z.; Yan, B.; Song, Y.; Chen, G.; Hou, L.; Crittenden, J. C. Biochar-Assisted Catalytic Pyrolysis of Oily Sludge to Attain Harmless Disposal and Residue Utilization for Soil Reclamation. *Environ. Sci. Technol.* 2023, *57*, 7063−7073.

(14) Vidonish, J. E.; Zygourakis, K.; Masiello, C. A.; Sabadell, G.; Alvarez, P. J. Thermal Treatment of Hydrocarbon-Impacted Soils: A Review of Technology Innovation for Sustainable Remediation. *Engineering* 2016b, *2*, 426−437.

(15) Hinchee, R. E. *In Situ Thermal Technologies for Site Remediation*; CRC Press, 1992.

(16) O'Brien, P. L.; DeSutter, T. M.; Casey, F. X. M.; Khan, E.; Wick, A. F. Thermal Remediation Alters Soil Properties - a Review. *J. Environ. Manage.* 2018, *206*, 826−835.

(17) O'Brien, P. L.; DeSutter, T. M.; Casey, F. X. M.; Wick, A. F.; Khan, E. Evaluation of Soil Function Following Remediation of Petroleum Hydrocarbons-a Review of Current Remediation Techniques. *Curr. Pollut. Rep.* 2017, *3*, 192−205.

(18) Denison, S. B.; Da Silva, P. D.; Koester, C. P.; Alvarez, P. J. J.; Zygourakis, K. Clays Play a Catalytic Role in Pyrolytic Treatment of Crude-Oil Contaminated Soils That Is Enhanced by Ion-Exchanged Transition Metals. *J. Hazard. Mater.* 2022, *437*, 129295.

(19) Mukherjee, J.; Sarofim, A. F.; Longwell, J. P. Polycyclic Aromatic Hydrocarbons from the High-Temperature Pyrolysis of Pyrene. *Combust. Flame* 1994, *96*, 191−200.

(20) Saito, H. H.; Bucala, V.; Howard, J. B.; Peters, W. A. Thermal Removal of Pyrene Contamination from Soil: Basic Studies and Environmental Health Implications. *Environ. Health Perspect.* 1998, *106*, 1097.

(21) Risoul, V.; Richter, H.; Lafleur, A. L.; Plummer, E. F.; Gilot, P.; Howard, J. B.; Peters, W. A. Effects of Temperature and Soil Components on Emissions from Pyrolysis of Pyrene-Contaminated Soil. *J. Hazard. Mater.* 2005, *126*, 128−140.

(22) O'Kelly, B. C.; Sivakumar, V. Water Content Determinations for Peat and Other Organic Soils Using the Oven-Drying Method. *Drying Technol.* 2014, *32*, 631−643.

(23) Enwezor, W. O. Soil Drying and Organic Matter Decomposition. *Plant Soil* 1967, *26*, 269−276.

(24) Jia, H. Z.; Zhao, J. C.; Li, L.; Li, X. Y.; Wang, C. Y. Transformation of Polycyclic Aromatic Hydrocarbons (PAHs) on Fe(III)-Modified Clay Minerals: Role of Molecular Chemistry and Clay Surface Properties. *Appl. Catal., B* 2014, *154−155*, 238−245.

(25) Talrose, V.; Stern, E. B.; Goncharova, A. A.; Messineva, N. A.; Trusova, N. V.; Efimkina, M. V. UV/Visible Spectra. In *NIST Standard Reference Database Number 69*; Linstrom, P. J., Mallard, W. G., Eds.; National Institute of Standards and Technology: Gaithersburg MD, 2017.

(26) Kresse, G.; Furthmüller, J. Efficiency of Ab-Initio Total Energy Calculations for Metals and Semiconductors Using a Plane-Wave Basis Set. *Comput. Mater. Sci.* 1996, *6*, 15−50.

(27) Perdew, J. P.; Burke, K.; Ernzerhof, M. Generalized Gradient Approximation Made Simple. *Phys. Rev. Lett.* 1996, *77*, 3865−3868.

(28) Blöchl, P. E. Projector Augmented-Wave Method. *Phys. Rev. B* 1994, *50*, 17953−17979.

(29) Kresse, G.; Joubert, D. From Ultrasoft Pseudopotentials to the Projector Augmented-Wave Method. *Phys. Rev. B* 1999, *59*, 1758−1775.

(30) Monkhorst, H. J.; Pack, J. D. Special Points for Brillouin-Zone Integrations. *Phys. Rev. B* 1976, *13*, 5188−5192.

(31) Grimme, S.; Antony, J.; Ehrlich, S.; Krieg, H. A Consistent and Accurate *Ab Initio* Parametrization of Density Functional Dispersion Correction (DFT-D) for the 94 Elements H-Pu. *J. Chem. Phys.* 2010, *132*, 154104.

(32) Viani, A.; Gualtieri, A. F.; Artioli, G. The Nature of Disorder in Montmorillonite by Simulation of X-Ray Powder Patterns. *Am. Mineral.* 2002, *87*, 966−975.

(33) Allen, G. C.; Curtis, M. T.; Hooper, A. J.; Tucker, P. M. X-Ray Photoelectron Spectroscopy of Iron−Oxygen Systems. *J. Chem. Soc., Dalton Trans.* 1974, 1525−1530.

(34) Biesinger, M. C.; Lau, L. W. M.; Gerson, A. R.; Smart, R. St. C. Resolving Surface Chemical States in XPS Analysis of First Row Transition Metals, Oxides and Hydroxides: Sc, Ti, V, Cu and Zn. *Appl. Surf. Sci.* 2010, *257*, 887−898.

(35) Nefedov, V. I.; Zhumadilov, K.; Kopytova, T. Yu. Comparison of the Chemical Shifts of X-Ray Electron and Auger Lines. *J. Struct. Chem.* 1978, *18*, 549−553.

(36) Mahadevi, A. S.; Sastry, G. N. Cation−π Interaction: Its Role and Relevance in Chemistry, Biology, and Material Science. *Chem. Rev.* 2013, *113*, 2100−2138.

(37) Zhang, W.; Cao, J.; Huang, H.; Zhang, R. Effect of Coexisting Lead and Phenanthrene on Their Individual Sorption on a Clayish Soil. *Soil Sediment Contam.* 2010, *19*, 322−337.

(38) Qu, X. L.; Liu, P.; Zhu, D. Q. Enhanced Sorption of Polycyclic Aromatic Hydrocarbons to Tetra-Alkyl Ammonium Modified Smectites via Cation-Pi Interactions. *Environ. Sci. Technol.* 2008, *42*, 1109−1116.

(39) Jia, H. Z.; Zhao, S.; Shi, Y. F.; Zhu, L. Y.; Wang, C. Y.; Sharma, V. K. Transformation of Polycyclic Aromatic Hydrocarbons and Formation of Environmentally Persistent Free Radicals on Modified Montmorillonite: The Role of Surface Metal Ions and Polycyclic Aromatic Hydrocarbon Molecular Properties. *Environ. Sci. Technol.* 2018, *52*, 5725−5733.

(40) Karimi-Lotfabad, S.; Pickard, M. A.; Gray, M. R. Reactions of Polynuclear Aromatic Hydrocarbons on Soil. *Environ. Sci. Technol.* 1996, *30*, 1145−1151.

(41) Liang, X.; Zhu, L. Z.; Zhuang, S. L. Sorption of Polycyclic Aromatic Hydrocarbons to Soils Enhanced by Heavy Metals: Perspective of Molecular Interactions. *J. Soils Sediments* 2016, *16*, 1509−1518.

(42) Zhang, W. H.; Zhuang, L. W.; Yuan, Y. A.; Tong, L. Z.; Tsang, D. C. W. Enhancement of Phenanthrene Adsorption on a Clayey Soil and Clay Minerals by Coexisting Lead or Cadmium. *Chemosphere* 2011, *83*, 302−310.

(43) Ni, Z.; Zhang, C.; Wang, Z. Q.; Zhao, S.; Fan, X. Y.; Jia, H. Z. Performance and Potential Mechanism of Transformation of Polycyclic Aromatic Hydrocarbons (PAHs) on Various Iron Oxides. *J. Hazard. Mater.* 2021, *403*, 123993.

(44) Saeedi, M.; Li, L. Y.; Grace, J. R. Effect of Organic Matter and Selected Heavy Metals on Sorption of Acenaphthene, Fluorene and Fluoranthene onto Various Clays and Clay Minerals. *Environ. Earth Sci.* 2018, *77*, 305.

(45) Gao, Y.; Guo, Y.; Zhang, H. Iron Modified Bentonite: Enhanced Adsorption Performance for Organic Pollutant and Its Regeneration by Heterogeneous Visible Light Photo-Fenton Process at Circumneutral PH. *J. Hazard. Mater.* 2016, *302*, 105−113.

(46) Hutson, N. D.; Gualdoni, D. J.; Yang, R. T. Synthesis and Characterization of the Microporosity of Ion-Exchanged Al_2O_3-Pillared Clays. *Chem. Mater.* 1998, *10*, 3707−3715.

(47) Senftle, T. P.; van Duin, A. C. T.; Janik, M. J. Role of Site Stability in Methane Activation on $Pd_xCe_{1-x}O_\delta$ Surfaces. *ACS Catal.* 2015, *5*, 6187−6199.

(48) Kumar, G.; Lau, S. L. J.; Krcha, M. D.; Janik, M. J. Correlation of Methane Activation and Oxide Catalyst Reducibility and Its Implications for Oxidative Coupling. *ACS Catal.* 2016, *6*, 1812−1821.

(49) Krcha, M. D.; Mayernick, A. D.; Janik, M. J. Periodic Trends of Oxygen Vacancy Formation and C−H Bond Activation over Transition Metal-Doped CeO2 (111) Surfaces. *J. Catal.* 2012, *293*, 103−115.

(50) Dias Da Silva, P.; Wong, M. S.; Zygourakis, K. JP-8 Desulfurization by CuNa-Y Zeolite at Elevated Temperatures Has Two Distinct Stages: Chemisorption Followed by Surface Reactions. *Ind. Eng. Chem. Res.* 2021, *60*, 14534−14546.

(51) King, D. L.; Faz, C. Desulfurization of Tier 2 Gasoline by Divalent Copper-Exchanged Zeolite Y. *Appl. Catal., A* 2006, *311*, 58−65.

(52) Sousa, J.; Pinto Da Silva, L. Modelling the Absorption Properties of Polycyclic Aromatic Hydrocarbons and Derivatives over Three European Cities by TD-DFT Calculations. *Sci. Total Environ.* 2019, *695*, 133881.

(53) Karcher, W.. *Spectral Atlas of Polycyclic Aromatic Compounds: Including Data on Occurrence and Biological Activity*; Dordrecht ; Boston : D. Reidel Pub. Co. for the Commission of the European Communities; Springer: Hingham, MA , 1985, Sold and distributed in the U.S.A. and Canada by Kluwer Academic Publishers.

(54) Gao, Y.; Zygourakis, K. Kinetic Study of the Pyrolytic Treatment of Petroleum Contaminated Soils. *Ind. Eng. Chem. Res.* 2019, *58*, 10829−10843.

(55) Gray, M. R.; McCaffrey, W. C. Role of Chain Reactions and Olefin Formation in Cracking, Hydroconversion, and Coking of Petroleum and Bitumen Fractions. *Energy Fuels* 2002, *16*, 756−766.

(56) Savage, P. E. Mechanisms and Kinetics Models for Hydrocarbon Pyrolysis. *J. Anal. Appl. Pyrolysis* 2000, *54*, 109−126.

(57) LaMarca, C.; Libanati, C.; Klein, M. T.; Cronauer, D. C. Enhancing Chain Transfer during Coal Liquefaction: A Model System Analysis. *Energy Fuels* 1993, *7*, 473−478.

(58) Van Speybroeck, V.; Van Neck, D.; Waroquier, M.; Wauters, S.; Saeys, M.; Marin, G. B. Ab Initio Study on Elementary Radical Reactions in Coke Formation. *Int. J. Quantum Chem.* 2003, *91*, 384−388.

(59) Savage, P. E.; Klein, M. T.; Kukes, S. G. Asphaltene Reaction Pathways. 1. Thermolysis. *Ind. Eng. Chem. Process Des. Dev.* 1985, *24*, 1169−1174.

(60) Yasar, M.; Trauth, D. M.; Klein, M. T. Asphaltene and Resid Pyrolysis. 2. The Effect of Reaction Environment on Pathways and Selectivities. *Energy Fuels* 2001, *15*, 504−509.

(61) Banerjee, D. K.; Laidler, K. J.; Nandi, B. N.; Patmore, D. J. Kinetic Studies of Coke Formation in Hydrocarbon Fractions of Heavy Crudes. *Fuel* 1986, *65*, 480−484.

(62) Alfadda, A. A.; Sallam, R. M. Reactive Oxygen Species in Health and Disease. *J. Biomed. Biotechnol.* 2012, *2012*, 1−14.

NOTE ADDED AFTER ASAP PUBLICATION

This paper posted ASAP on September 9, 2023 with production errors. The paper was corrected and reposted on September 11, 2023.